



# Deep Western Boundary Current variability in the subtropical northwest Atlantic Ocean during marine isotope stages 12–10

Ian R. Hall and Julia Becker

*School of Earth, Ocean and Planetary Science, Cardiff University, Main Building, Park Place, Cardiff CF10 3YE, UK (hall@cardiff.ac.uk)*

[1] High-resolution (125–500 year temporal resolution) sortable silt mean grain size data of subtropical northwest Atlantic Ocean Drilling Program (ODP) Leg 172, Site 1061, monitor fluctuations of the Deep Western Boundary Current (DWBC) throughout marine oxygen isotope stages (MIS) 12–10 (330–460 kyr) in great detail. Comparison with foraminiferal stable isotope data from the same site and ODP Site 1063 (Bermuda Rise, data of Poli et al. (2000)) shows that the DWBC shoals during glacial times in relation to a reduced North Atlantic Deep Water production and increased advection of southern ocean waters. Superimposed fluctuations in the flow speed/position of the DWBC at a semiprecession scale are persistent throughout MIS 10–12 and independent of the glacial state. Additional millennial-scale variations in DWBC flow speed parallel surface water cooling events and ice-rafted debris episodes especially at the transition of MIS 11/10, indicating the sensitivity of deep current flow variations to changes in the surface water conditions. These millennial-scale variations are amplified when benthic foraminiferal  $\delta^{18}\text{O}$  values exceed  $\sim 3.8\text{‰}$  and may be related to the transition of an ice volume threshold where climate variability is possibly amplified by feedback mechanisms associated with ice sheet growth.

**Components:** 7613 words, 6 figures.

**Keywords:** Atlantic thermohaline circulation; Deep Western Boundary Current; Blake-Bahama Outer Ridge; ODP Leg 172; sortable silt mean grain size.

**Index Terms:** 4576 Oceanography: Physical: Western boundary currents; 4962 Paleooceanography: Thermohaline.

**Received** 26 October 2006; **Revised** 7 February 2007; **Accepted** 8 March 2007; **Published** 26 June 2007.

Hall, I. R., and J. Becker (2007), Deep Western Boundary Current variability in the subtropical northwest Atlantic Ocean during marine isotope stages 12–10, *Geochem. Geophys. Geosyst.*, 8, Q06013, doi:10.1029/2006GC001518.

## 1. Introduction

[2] The oceans will play a key role in shaping future climate that can be better understood through the study of suitable environmental analogues in the geological record. As such, marine isotope stage (MIS) 11 (428–360 kyr B.P.) is perhaps the closest equivalent to the Holocene as the orbital configuration, and thus insolation forc-

ing of the Earth's climate system, were similar [Berger and Loutre, 1991; Loutre and Berger, 2003]. In addition, atmospheric greenhouse gases were also comparable to the preindustrial values [Petit et al., 1999; EPICA Community Members, 2004]. Despite growing interest our understanding of MIS 11 is still patchy [e.g., de Abreu et al., 2005]. One uncertainty lies in the intensity and stability of North Atlantic Deep Water (NADW)



production and its possible role in promoting the longevity of the MIS 11 interval.

[3] A key region to study the variability of NADW is the Blake-Bahama Region in the western equatorial Atlantic Ocean (Figure 1), where as a major component of the global thermohaline circulation, the Deep Western Boundary Current (DWBC) carries recently ventilated waters (i.e., NADW) equatorward. The present-day volume transport of this deep current is estimated to be  $\sim 17$  Sv in the subpolar Atlantic Ocean [e.g., *McCartney and Talley*, 1984; *Schmitz and McCartney*, 1993] with another 17 Sv being added from an extended cyclonic gyre in the western equatorial Atlantic Ocean, reaching from the equator to about  $30^\circ\text{N}$  [*Schmitz and McCartney*, 1993]. Therefore the total equatorward transport of northern source deep water in the DWBC is suggested to be  $\sim 34$  Sv south of  $30^\circ\text{N}$ .

[4] The 700 km long Blake-Bahama Outer Ridge (BBOR,  $32^\circ\text{N}$ ,  $76^\circ\text{W}$ ) is a sedimentary drift body that extends from the continental margin of North America, south of Cape Hatteras and north of the Bahama Islands (Figure 1). Sloping to the southeast the BBOR extends from  $\sim 2,000$  m water depth down on to the Hatteras Abyssal Plain at about 5,000 m water depth. The sediment drift has developed through the interaction of the strong southward flowing DWBC with the northward flowing Gulf Stream (Florida Current) as it detaches from the continental shelf [*Bryan*, 1970; *Stahr and Sanford*, 1999]. Sedimentation rates reach up to  $\sim 60$  cm kyr<sup>-1</sup> with terrigenous sediments being supplied both by material eroded from the continental margin to the north and being transported south by the DWBC [*Ewing et al.*, 1966; *Heezen et al.*, 1966; *Laine et al.*, 1994] and by material transported downslope from the Blake Plateau [*Bryan*, 1970; *McCave and Tucholke*, 1986].

[5] Sedimentation on the BBOR is affected by the different water masses of the DWBC and considerable effort has been directed at investigating the modern flow characteristics in the BBOR region [*Haskell and Johnson*, 1993; *Stahr and Sanford*, 1999]. The DWBC complex over the BBOR is subdivided into four main water masses [*Stahr and Sanford*, 1999]: a shallow component of Labrador Seawater (SLSW; 1,000–1,800 m water depth), underlain by LSW (1,400–2,800 m water depth), lower North Atlantic Deep Water (LNADW; 2,500–4,100 m water depth) and deep Bottom Water (BW;  $>3,400$  m water depth to the bottom).

Only this latter water mass contains a significant component ( $\sim 10$ – $16\%$ ) of water with a southern source (Antarctic Bottom Water, AABW). This southern ocean source water has been recirculated in a cyclonic gyre north of the BBOR [*Amos et al.*, 1971; *Stahr and Sanford*, 1999], and therefore has the same flow direction at the BBOR as the overlying LNADW (Figure 1) [*Weatherly and Kelley*, 1984].

[6] The DWBC is strongly constrained by the bottom topography, with the most recently ventilated water located predominantly adjacent to the steepest part of the continental slope [*Johns et al.*, 1997]. A high-velocity core of the DWBC follows the bathymetric contour around BBOR, deepening from  $\sim 3,500$  m water depth near the upstream origin of the BBOR to  $\sim 4,100$  m, downstream along the eastern flank of the ridge [*Stahr and Sanford*, 1999]. The depth range of the BBOR water masses given above overlie each other reflecting this deepening of the DWBC flow along the ridge crest [*Stahr and Sanford*, 1999].

[7] The strength and flow characteristics of the DWBC are known to have varied in space (depth) and time, in response to changes in source water production. Previous studies have utilized grain size analyses in order to reconstruct these changes on millennial to Milankovitch timescales [e.g., *Johnson et al.*, 1988; *Haskell et al.*, 1991; *Bianchi et al.*, 2001; *Yokokawa and Franz*, 2002]. *Haskell et al.* [1991] investigated changes in the DWBC flow on the BBOR since the Last Glacial Maximum (LGM) using four cores recovered from 2,650 to 3,818 m water depths. Their results show that the fast flowing core of the DWBC was shallower than 2900 m prior to  $\sim 14$  kyr B.P. back to the LGM. *Bianchi et al.* [2001] combined grain size data with benthic  $\delta^{13}\text{C}$  data from ODP Site 1060 (3,480 m water depth) and Site 1062 (4,760 m water depth) and reconstructed the intensity and position of the fast flowing core of the DWBC between 130–110 kyr (MIS 6-5d), while *Yokokawa and Franz* [2002] integrated grain size measurements and magnetic properties for the interval 350–250 kyr (MIS 10.2–8.3) using ODP Sites 1055–1062 (1,800 m to 4,760 m water depths). These data show that the core of the DWBC is located at a water depth  $>3,000$  m during interglacial periods shoaling to around 2,500–3,000 m water depth during glacial periods.

[8] Here we focus on changes in the near bottom flow speed and hydrography of the DWBC recorded at ODP Leg 172, Site 1061 ( $29^\circ 59'\text{N}$ ,

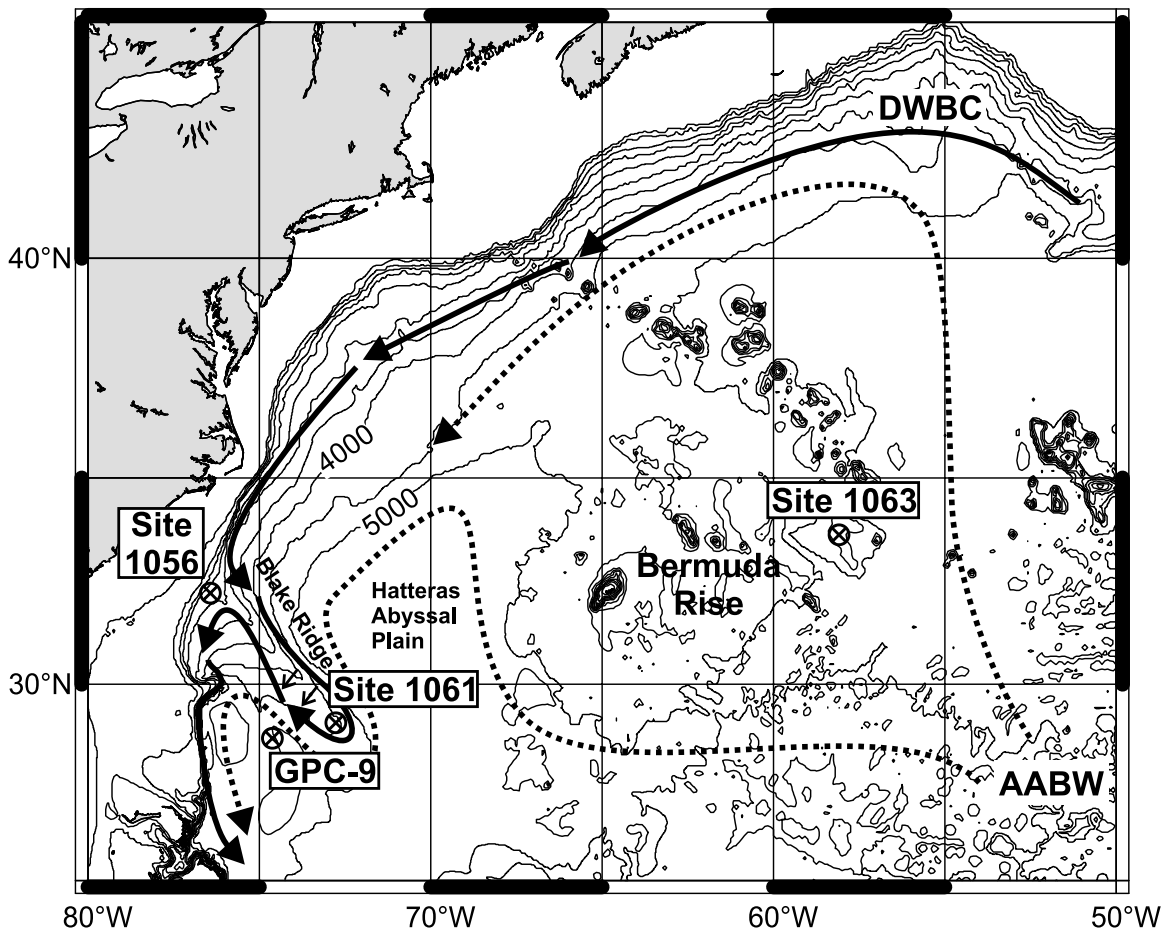


**Figure 1.** General bathymetric map showing positions of ODP Leg 172 Sites 1061, 1056, and 1063, along with core KN31-GPC-9. The schematic flow of the Deep Western Boundary Current is indicated by the solid arrow [after *Stahr and Sanford, 1999*], while the flow of recirculating Antarctic Bottom Water is shown by the dotted arrows [after *Weatherly and Kelley, 1984*].

73°36'W; 4,047 m water depth, Figure 1) on the deep BBOR in the northwestern Atlantic Ocean. Grain size (sortable silt mean ( $\overline{SS}$ )) and foraminiferal stable isotope ( $\delta^{18}\text{O}$  and  $\delta^{13}\text{C}$ ) data are used in conjunction with previously published planktonic foraminiferal stable isotope data from Site 1056 [*Chaisson et al., 2002*] on BBOR (32°29'N, 76°20'W; 2,166 m water depth) and benthic foraminiferal stable isotope data from Site 1063 [*Poli et al., 2000*] (33°41'N, 57°37'W; 4,595 m water depth) on the Bermuda Rise to investigate paleoceanographic changes during MIS 12–10 (450–340 kyr). In contrast to the foraminiferal stable isotope record, which is patchy as suitable benthic foraminifera were not found in all samples due to both dissolution of the calcareous shells and dilution at this high sediment deposition rate site, the  $\overline{SS}$  record is continuous, since terrigenous sediments are ubiquitous through the sediment core.

This allows us to obtain an uninterrupted high-resolution record of paleocurrent speed through MIS 12–10, likely the reflection of LNADW ventilation.

## 2. Material and Methods

[9] During ODP Leg 172 a depth transect (1,800 to 4,800 m water depth) was drilled along the BBOR in order to document rapid changes in climate and ocean circulation. The recovered sediments are mainly composed of alternating beds of dark greenish-gray terrigenous silt, clay-dominated sediments and light greenish-gray carbonate (nannofossil)-rich sediments [*Shipboard Scientific Party, 1998*]. These alterations are reflected in the sedimentary color and magnetic susceptibility logs and have been shown to vary at a glacial-interglacial timescale [*Grützner et al., 2002*].

[10] ODP Site 1061 was recovered at 4,047 m water depth (Figure 1), on the crest of the Blake Ridge above the present-day fast flowing core of the DWBC [Stahr and Sanford, 1999; Bianchi et al., 2001]. MIS 11 is clearly identified in the magnetic susceptibility record [Shipboard Scientific Party, 1998] at a depth of 100.71–116.53 mcd (meter composite depth) with implied sedimentation rates of  $\sim 27$  cm kyr<sup>-1</sup> [Grützner et al., 2002]. In order to investigate the full evolution of MIS 11 in detail, the interval 96.91–121.30 mcd, representing MIS 10–12, was sampled every 5 cm following the composite depth profile [Shipboard Scientific Party, 1998]. Additionally, the interval 26.40–37.44 mcd (61.5–129.5 kyr) comprising MIS 5 was sampled on a lower 10-cm resolution in order to reconcile DWBC variability as recorded at Site 1061 with previously published records of benthic  $\delta^{13}\text{C}$  deep ocean ventilation. Samples from both time intervals were wet sieved through 63, 150 and 215  $\mu\text{m}$  sieves, all fractions were preserved, dried and weighed following the sample preparation procedures as described by Bianchi et al. [2001]. The percent carbonate content of the sediment was estimated using the inorganic carbon content determined by a Perkin Elmer 2400 elemental analyzer following the methods of King et al. [1998] lab F.

[11] In order to reconstruct water mass properties during MIS 11, stable isotope ( $\delta^{18}\text{O}$  and  $\delta^{13}\text{C}$ ) analysis were carried out on benthic and planktonic foraminifera wherever abundant specimens were available in the sample. For isotopic measurements  $\sim 10$  specimens of the planktonic foraminifera species *Globigerinoides ruber* (white) and 2–3 specimens of the benthic foraminifera species *Cibicides wuellerstorfi* or *Uvigerina peregrina* were selected from the  $>150$ – $250$   $\mu\text{m}$  fraction. All analyses were performed using a Finnigan MAT252 mass spectrometer with automated carbonate preparation device at Cardiff University stable isotope facility. Stable isotope results were calibrated to the PDB scale by international standard NBS19. The analytical precision is better than  $\pm 0.08\text{‰}$  and  $\pm 0.05\text{‰}$  for  $\delta^{18}\text{O}$  and  $\delta^{13}\text{C}$ , respectively. Oxygen isotope values of *C. wuellerstorfi* were corrected by  $+0.64\text{‰}$  to bring them into agreement with ambient seawater [Shackleton and Opdyke, 1973; Shackleton and Hall, 1984]. The  $\delta^{13}\text{C}$  of *U. peregrina* were adjusted by  $+0.9\text{‰}$  to correct for vital effect [Shackleton and Hall, 1984].

[12] In order to infer past paleocurrent intensity we employ the mean grain size of the terrigenous 10–

63  $\mu\text{m}$  fraction, known as the sortable silt mean ( $\overline{\text{SS}}$ ), that provides an estimate of relative changes in near-bottom flow intensity of the depositing paleocurrent [McCave et al., 1995; McCave and Hall, 2006] with a higher value representing stronger mean near-bottom current speeds and vice versa. Prior to analysis carbonate was removed from the fine fraction ( $<63$   $\mu\text{m}$ ) by dissolution in 1M acetic acid solution (48h at room temperature). Subsequently, biogenic opal was removed by digestion in 2M sodium carbonate solution (5h at 85°C). All  $\overline{\text{SS}}$  measurements were made using a Coulter Multisizer III as detailed by Bianchi et al. [1999]. For the MIS 10–12 interval, additional grain size measurements were undertaken on a 15 cm resolution using a Sedigraph 5100 in order to determine the sortable silt abundance (SS%) and the silt/clay ratio. The SS% varies in the range of 5–10% enabling the determination of the  $\overline{\text{SS}}$  with an analytical error of  $<2\%$  [Bianchi et al., 1999].

[13] Spectral analysis of the MIS 12–10  $\overline{\text{SS}}$  record of Site 1061 was carried out using the MC\_CLEAN (v. 2.0) routine of Heslop and Dekkers [2002], which is based on the CLEAN algorithm of Roberts et al. [1987]. The routine allows frequency information to be extracted directly from an unevenly spaced time series. In addition to CLEAN, Monte Carlo methods for different types of noise (here red noise) allow the generation of a suite of slightly varying spectra from the (single) input signal. The differences between these spectra define the confidence interval around the mean spectrum. Additionally, we applied wavelet analysis using the MATLAB routine of Torrence and Compo [1998] and band pass filtering using the AnalySeries program [Paillard et al., 1996]. The band filters and widths were chosen according to the central frequencies of the significant peaks in spectral power.

[14] The Site 1061 data presented in this paper are available as an electronic data supplement (see auxiliary material<sup>1</sup> Table S1).

## 2.1. ODP Site 1061 Chronology

[15] The generally low abundance of benthic foraminifera in the MIS 10–12 interval at Site 1061 did not allow establishing a continuous benthic  $\delta^{18}\text{O}$  stratigraphy. Therefore the age model is based entirely on the graphical correlation of the Site 1061  $\text{CaCO}_3$  abundance record with the  $\text{CaCO}_3$

<sup>1</sup>Auxiliary material data sets are available at <ftp://ftp.agu.org/apend/gc/2006gc001518>. Other auxiliary material files are in the HTML.

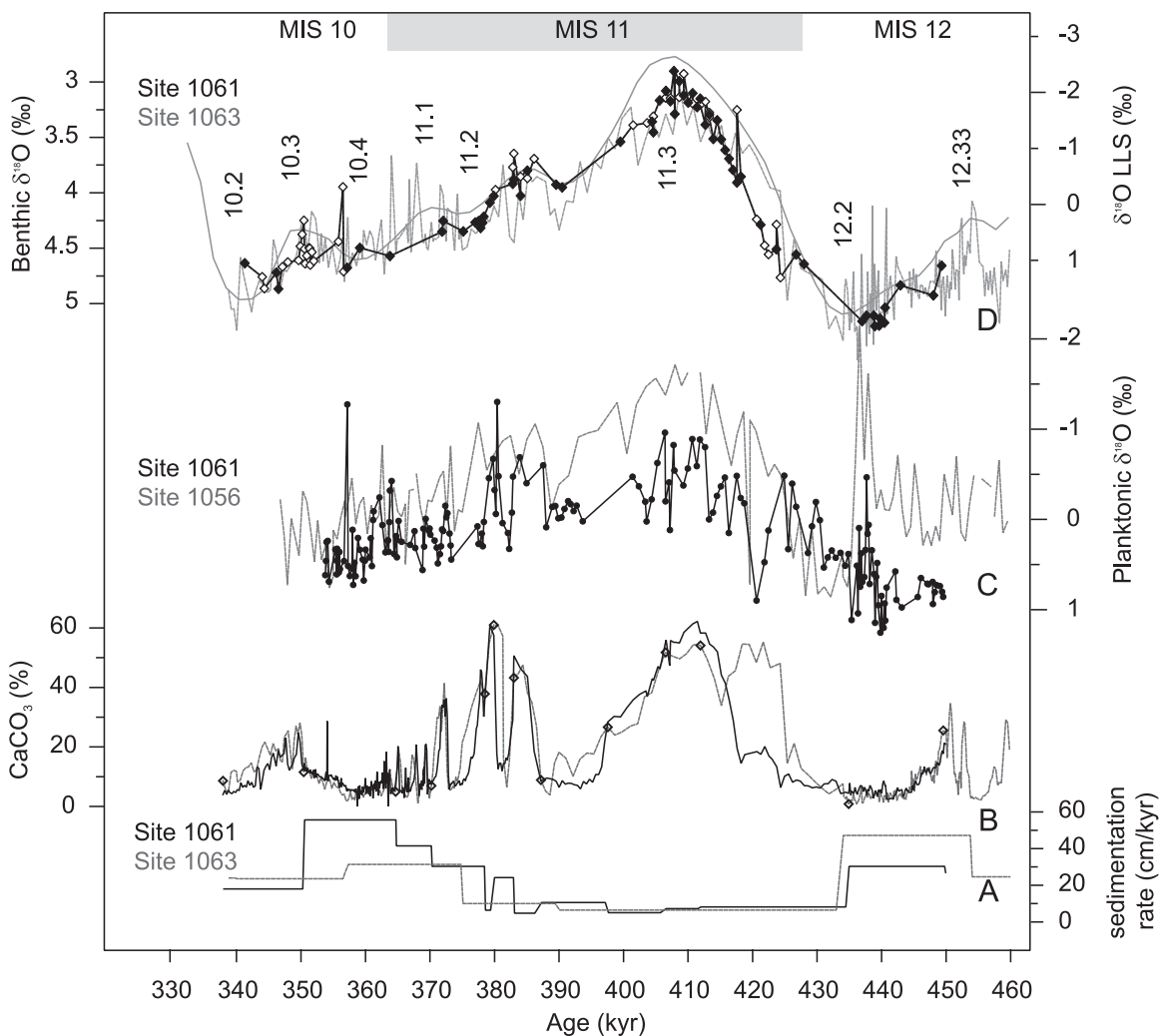


**Figure 2.** Chronology of ODP Site 1061. (a) Sedimentation rates for Site 1063 (gray stipple line) [Poli *et al.*, 2000] and Site 1061 (solid black line). (b) CaCO<sub>3</sub> percentage of Site 1063 (gray stipple line; data of Poli *et al.* [2000]) and Site 1061 (solid black line) with age correlation points indicated (open diamonds). (c) Planktonic  $\delta^{18}\text{O}$  from Site 1056 measured on *G. sacculifer* (gray stipple line) [Chaisson *et al.*, 2002] and  $\delta^{18}\text{O}$  from Site 1061 measured on *G. ruber*. (d) Benthic  $\delta^{18}\text{O}$  of Site 1063 (gray stipple line; data of Poli *et al.* [2000]) and Site 1061 (black stipple line) in relation to the low-latitude stack (LLS) of Bassinot *et al.* [1994] with MIS labeled. Benthic  $\delta^{18}\text{O}$  of Site 1063 is measured on *Cibicidoides wuellerstorfi*, and Site 1061 is measured on *C. wuellerstorfi* (black diamonds) and *Uvigerina peregriana* (open diamonds). MIS 11 is indicated by the gray shading.

record of ODP Site 1063 at Bermuda Rise [Poli *et al.*, 2000] (Figure 2). The Poli *et al.* [2000] age scale of Site 1063 was developed by tuning the benthic  $\delta^{18}\text{O}$  record to the astronomically calibrated low-latitude stack (LLS) of Bassinot *et al.* [1994]. Both CaCO<sub>3</sub> abundance records show similar variations during MIS 10–12, ranging from 2.5 wt% in the glacials to 60 wt% during MIS 11, with distinct CaCO<sub>3</sub> maxima during the peak interglacial and early MIS 10. Only during early MIS 11 are CaCO<sub>3</sub> values at Site 1061 lower than those of

Site 1063, in agreement with CaCO<sub>3</sub> record of ODP Site 1056 at BBOR [Chaisson *et al.*, 2002]. In total 13 tie points were set to establish the correlation ( $r = 0.79$ ) and ages were linearly interpolated in between. Comparison of the benthic  $\delta^{18}\text{O}$  records of Site 1061 and Site 1063 [Poli *et al.*, 2000] supports the age calibration especially across the MIS 12/11 transition (Figure 2). Benthic  $\delta^{18}\text{O}$  values at Site 1061 are  $\sim 4.5\text{‰}$  during MIS 12 and  $\sim 3\text{‰}$  in the MIS 11.3 interglacial, with a glacial-interglacial (G-I) amplitude in agreement

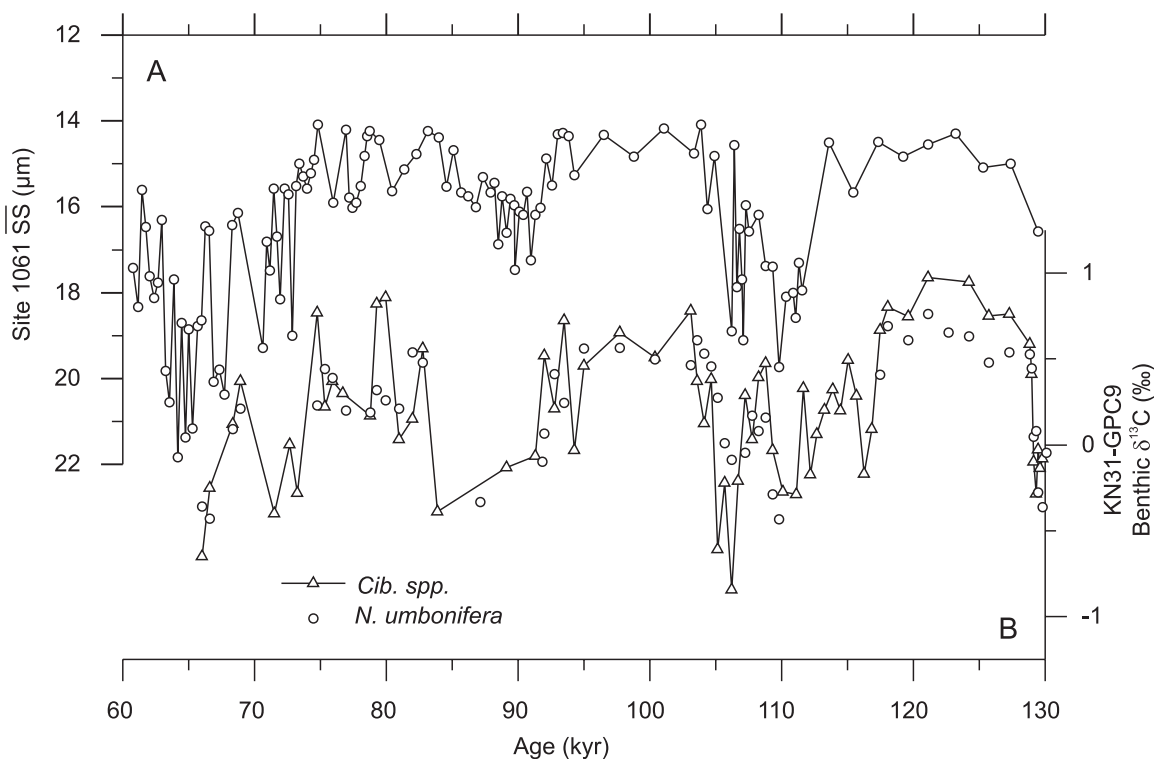


**Figure 3.** (a) Site 1061  $\overline{SS}$  grain size ( $\mu\text{m}$ ) versus age (kyr) during MIS 5. Note reversed axis. (b) Benthic  $\delta^{13}\text{C}$  of Site KN31-GPC9 with open circles indicating measurements on *N. umbonifera* and open triangles indicating measurements on *Cibicidoides* spp. [Keigwin *et al.*, 1994].

with Site 1063. Marine isotope stages as indicated in the LLS [Bassinot *et al.*, 1994] are partly recognized in the benthic  $\delta^{18}\text{O}$  of Site 1061. The age correlation is further confirmed by the  $\delta^{18}\text{O}$  measurements on the planktonic foraminifera *G. ruber* ( $\delta^{18}\text{O}_{G.ruber}$ ).  $\delta^{18}\text{O}_{G.ruber}$  values at Site 1061 are slightly higher than those of planktonic foraminifera *Globigerinoides sacculifer* ( $\delta^{18}\text{O}_{G.sacc}$ ) at Site 1056 [Chaisson *et al.*, 2002], ranging from 1‰ in the glacial to minimum values of  $-1$ ‰ during MIS 11. Both records show similar lower amplitude variations with 5–8 kyr spacing during MIS 11 and more rapid variations ( $\sim 2$  kyr) during the glacial intervals. The landmark excursion toward light  $\delta^{18}\text{O}$  values at  $\sim 440$  kyr is well resolved in both records.

[16] The Site 1061 age model results in sedimentation rates of up to  $40 \text{ cm kyr}^{-1}$  during the glacials MIS 10 and 12 and  $10 \text{ cm kyr}^{-1}$  during early MIS 11, closely matching those of Site 1063 (Figure 2). At our 5 cm sampling interval this represents a temporal spacing of between 125 and 500 years respectively.

[17] The chronology for the low-resolution interval around MIS 5 is based on the correlation of the Site 1061  $\text{CaCO}_3$  with the  $\text{CaCO}_3$  of nearby core KN31-GPC-9 [Keigwin *et al.*, 1994] (see auxiliary material Figures S1 and Table S1).

## 2.2. Framework for Interpretation of Site 1061 Paleocurrent Reconstructions

[18] From modern hydrographic investigations, it is apparent that there is an association between the spatial extent of NADW and strong deep water circulation [Stahr and Sanford, 1999]. However, the geochemical signal of NADW is more likely to be spatially extensive whereas the flow intensity of NADW will be more variable due to the nature of the DWBC and its interactions with local bathymetry. Such caveats may in part account for the fairly limited amount of clear evidence for consistent behavior between sedimentological flow speed and geochemical hydrographic proxies [McCave and Hall, 2006]. However, the link between deep water circulation and climate is clearly demonstrated by the benthic  $\delta^{13}\text{C}$  record from core GPC-9 [Keigwin *et al.*, 1994] recovered on the Bahama Outer Ridge in the subtropical Northwest Atlantic



Ocean at 4,758 m depth (Figure 1). The low-resolution  $\overline{SS}$  record of Site 1061 (Figure 3; note reversed scale), demonstrates a close similarity to the benthic  $\delta^{13}C$  data from GPC-9 in the MIS 5 interval. From  $\sim 130$  kyr onward the correlation is unambiguous and demonstrates a strong relationship between ventilation of LNADW and the DWBC near bottom flow speed at Site 1061. The mean grain size decreases with increasing NADW production/presence at GPC-9, which is fully consistent with the structure of the DWBC in this region as illustrated by modern hydrographic data [Stahr and Sanford, 1999] and similar observations at shallower ODP Leg 172 sites during MIS 5 [Bianchi *et al.*, 2001]. As the fast flowing core of the current presently lies at depths greater than Site 1061, a reduction, thus shoaling, of LNADW accompanied by the increased contribution of southern source water would result in an upward migration of the DWBC and an increase in the flow vigor at Site 1061. This is supported by the changing sedimentation rates, which increase substantially during the phases of reduced LNADW production (Figure 2).

### 3. Results

[19] Sortable silt mean grain sizes during MIS 12 average  $15 \mu\text{m}$  with superimposed millennial-scale ( $\sim 2$  kyr) flow variability of  $\pm 1 \mu\text{m}$  around the mean. During early MIS 11,  $\overline{SS}$  values decrease to an average of  $14.7 \mu\text{m}$  with variations of similar amplitude spaced 9–11 kyr apart. During late MIS 11 (above 397 kyr) flow speeds again increase to average values of  $15 \mu\text{m}$  but show much higher amplitude ( $\pm 2 \mu\text{m}$ ) millennial-scale (3–5 kyr) variations (Figure 4). Coincident with the increase in flow speeds after 397 kyr, the silt/clay ratio increases from 0.6 to maximum values of 1.5 (Figure 4), indicating a general coarsening of the sediment, clearly preceding the increase in sedimentation rate around the MIS 11/10 transition by  $\sim 10$  kyr. Furthermore, silt/clay ratios display a set of distinct peaks after 397 kyr, which are spaced  $\sim 5$  kyr apart and correlate with high  $\overline{SS}$  values and decreased  $\text{CaCO}_3$  and benthic  $\delta^{13}C$  at Site 1063 [Poli *et al.*, 2000] (Figure 4), indicating a change in water mass properties associated with the vertical migration of the DWBC and increased presence of nutrient-rich and more corrosive AABW at these times. Given the good agreement between the  $\text{CaCO}_3$  and benthic  $\delta^{13}C$  records of Site 1061 and Site 1063 (Figure 4), we assume a similar hydrographic interpretation. As shown above at the

depth of Site 1061 increased  $\overline{SS}$  values are indicative of a shoaling of the deeper fast flowing DWBC core along the BBOR and thus a closer position of the DWBC core relative to Site 1061. This shoaling of the DWBC is associated with a reduction of the thermohaline circulation and LNADW production. The relatively high  $\overline{SS}$  values at Site 1061 during MIS 12 and MIS 10 are in agreement with a glacial “shallow” mode, where increased  $\overline{SS}$  values reflect a flow axis of the DWBC closer to the site. On the contrary, lower  $\overline{SS}$  values during MIS 11 are consistent with a “deep” mode and the fast flowing DWBC axis being located deeper than Site 1061.

[20] Spectral analysis of the  $\overline{SS}$  reveals maximum concentration of power above the 90% confidence level at or near periodicities of 90–, 34–, 9.5–, 5.4–, 4.2– and 2.6 kyr in agreement with wavelet results (Figures 5a and 5c). The wave map indicates maximum variance at the half precession during early MIS 11 and after 370 kyr. Increasing spectral variance at the low periodicities (5–2.6 kyr) is observed during late MIS 11 (397–360 kyr). Time resolution is high in the entire interval so that the increase toward lower periodicities after 397 kyr is not related to the increase in sedimentation rate. Furthermore, spectral analysis results are supported by the filter outputs located at the central frequencies of maximum variance (Figure 5b). The amplitude of the 9.5 kyr filter output is slightly larger during early MIS 11 and after 370 kyr, while amplitudes of the 5.4 kyr filter output (and the 4 and 2.6 kyr outputs not shown) are at maximum during late MIS 11.

## 4. Discussion

### 4.1. Variability of DWBC During MIS 12–10

[21] Site 1061 sedimentary properties and benthic stable isotope data suggest that the DWBC at the BBOR operated in three different modes during MIS 10–12: in a shallow mode during peak glacial MIS 12, a deep mode during peak interglacial MIS 11.3 and a variable mode toward MIS 10 (after 397 kyr). The shallow mode during late MIS 12 is characterized by small amplitude variations around high  $\overline{SS}$  values being in agreement with a relatively stable shallow/fast flowing DWBC. Benthic  $\delta^{13}C$  values indicate a high contribution of southern origin water confirming a shallow positioning of the DWBC at Site 1061. High-amplitude millennial-scale stadial-interstadial type of variations as

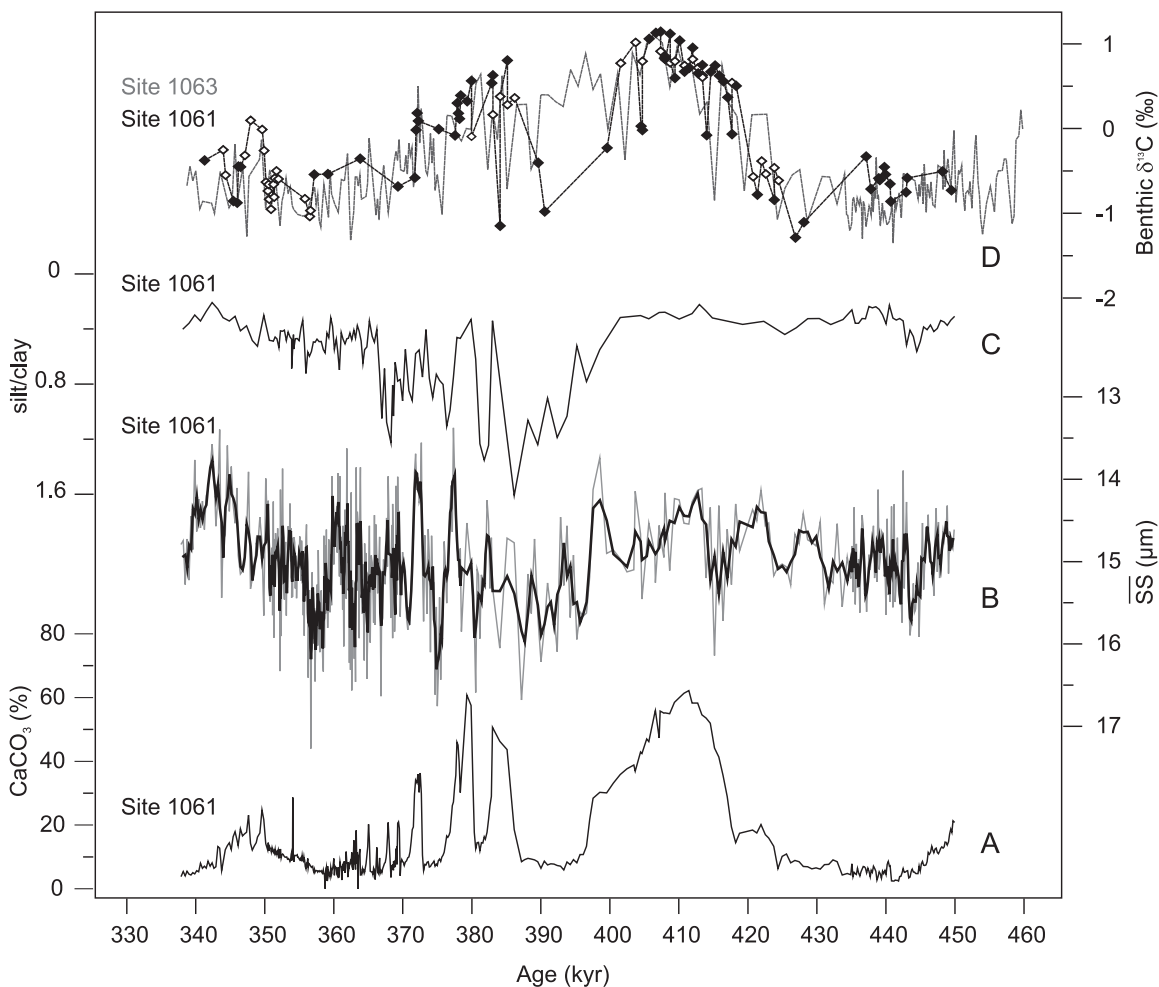


**Figure 4.** (a) Site 1061 percentage  $\text{CaCO}_3$ . (b) Site 1061  $\overline{\text{SS}}$  grain size (gray line) with overlain 3pt moving average (note reversed axis). (c) Site 1061 silt/clay ratio. Note reversed axis. (d) Benthic  $\delta^{13}\text{C}$  of Site 1063 (gray stipple line; data of *Poli et al.* [2000]) and Site 1061 (black stipple line) versus age (kyr). Benthic  $\delta^{13}\text{C}$  of Site 1063 is measured on *Cibicidoides wuellerstorfi*, and Site 1061 is measured on *C. wuellerstorfi* (black diamonds) and *Uvigerina peregrina* (open diamonds).

observed in the benthic  $\delta^{13}\text{C}$  of Site 1063 during the early MIS 12 are absent during this later interval [*Poli et al.*, 2000], suggesting that NADW formation was stable at low to intermediate levels.

[22] In contrast to the “shallow” the “deep” DWBC mode during early MIS 11 is characterized by on average lower  $\overline{\text{SS}}$  values at Site 1061, suggesting a deeper flowing DWBC and increased production of LNADW. Benthic  $\delta^{13}\text{C}$  values indicate a decreasing influence of southern ocean water with NADW becoming the dominant deep water mass during peak interglacial MIS 11.3. This is in agreement with a vigorous NADW formation during MIS 11. However, our proxy records indicate

that the transition from a “shallow” to a “deep” DWBC at the MIS 12 deglaciation ( $\sim 430$  kyr) was not rapid but instead punctuated by at least two recursions toward faster/shallower DWBC flow  $\sim 425$  kyr and 420 kyr. Each of these excursions is accompanied by low benthic  $\delta^{13}\text{C}$  and  $\text{CaCO}_3$  values, indicating short episodes of increased AABW contribution/decreased NADW production. The observed discrepancy between the Site 1061 and Site 1063  $\text{CaCO}_3$  records during  $\sim 420$ –415 kyr, with the deeper Site 1063 showing a marked  $\text{CaCO}_3$  preservation spike is probably related to a decrease in the intermediate-to deep  $\Delta^{13}\text{C}$  gradient during the termination and subsequent carbonate saturation increase in deep water

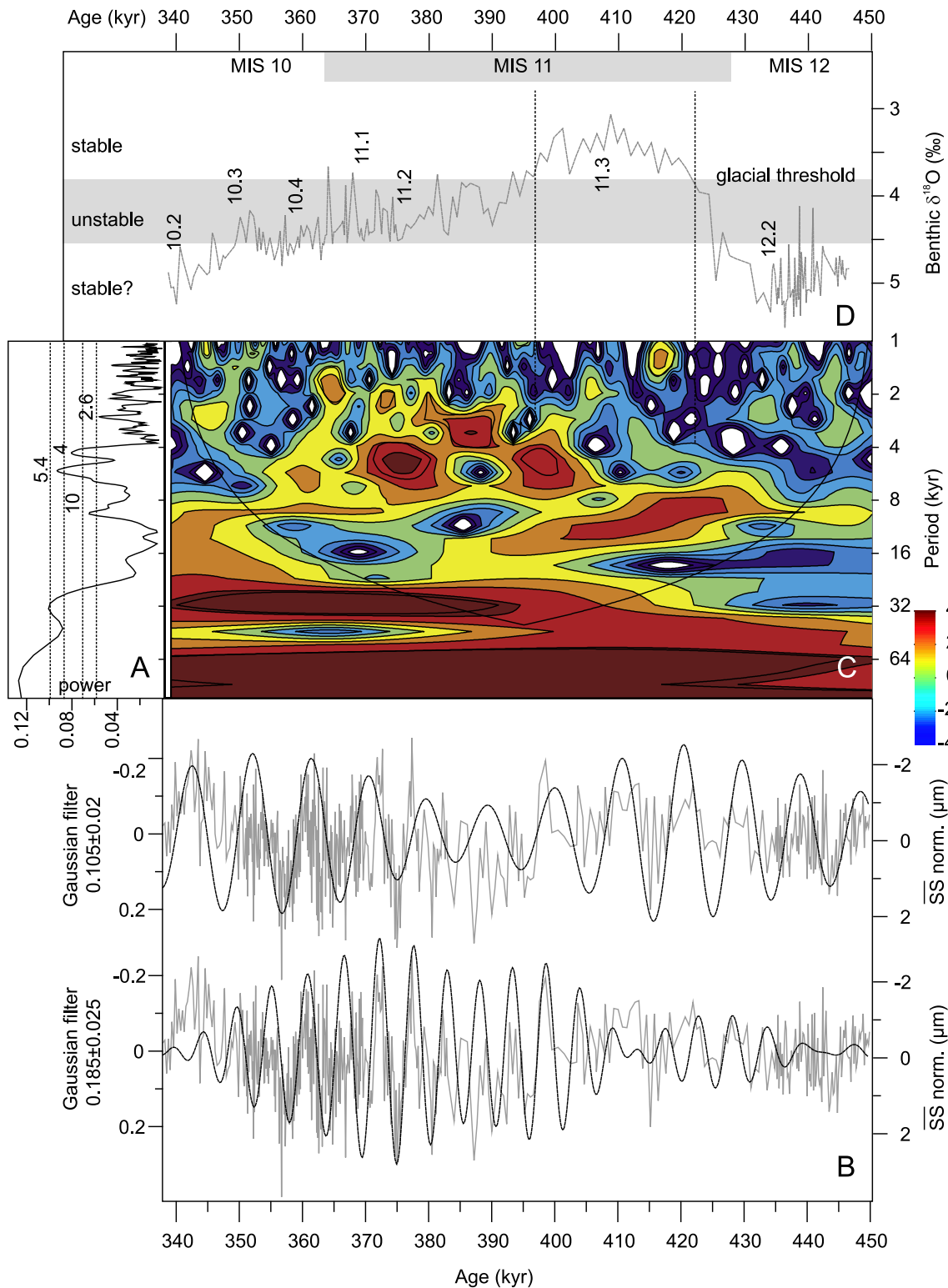


**Figure 5.** (a) Power spectrum (left-hand side) with 90%, 95%, 98%, and 99% confidence intervals (stippled lines) of Site 1061 SS record. The main periodicities are indicated in the spectrum. (b) Site 1061 normalized SS record versus age (kyr) overlain by Gaussian filters (stippled lines) with central frequency at  $0.185 \pm 0.025$  cycles/kyr ( $4.7 < 5.4 < 6.2$  kyr) and  $0.105 \pm 0.02$  cycles/kyr ( $8 < 9.5 < 11.7$  kyr). (c) Waveplot of the Site 1061 SS record versus periodicity (kyr). (d) Site 1063 benthic  $\delta^{18}\text{O}$  record [Poli *et al.*, 2000] versus age. Labels indicate MIS. Upper gray bar indicates the time interval of MIS 11. Lower gray horizontal bar indicates the interval of increased high-frequency variability between 3.8 and 4.5‰.

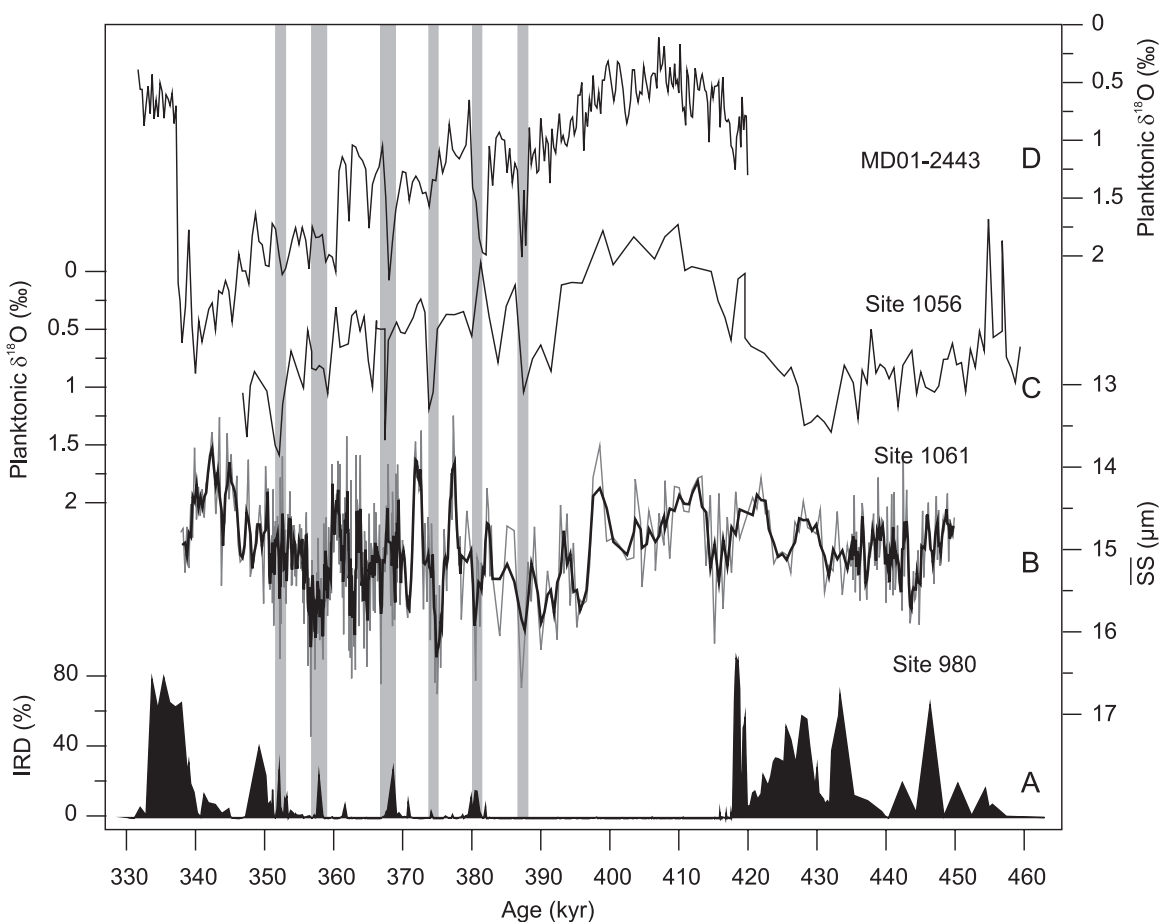


**Figure 6.** (a) ODP Site 980 ice-rafted debris abundance [McManus *et al.*, 1999]. (b) Site 1061  $\overline{SS}$  grain size ( $\mu\text{m}$ ). Note reversed scale. (c) Planktonic  $\delta^{18}\text{O}$  from Site 1056 measured on *N. dutertrei* [Chaisson *et al.*, 2002] and core MD01-2443 measured on *G. bulloides* [de Abreu *et al.*, 2005]. Gray shadings indicate episodes of cold surface waters as indicated in the planktonic  $\delta^{18}\text{O}$  of Site 1056 and MD01-2443.

as  $\text{CO}_2$  is redistributed out of the deep ocean [Hodell *et al.*, 2003].

[23] In contrast to the slow reorganization of the DWBC at the deglaciation,  $\overline{SS}$  and silt/clay ratios indicate a rapid reorganization toward a shallow/fast flowing DWBC at  $\sim 397$  kyr. Coincident with this shift decreasing  $\text{CaCO}_3$  contents suggest an increased contribution of southern source water. Superimposed high-amplitude changes in  $\overline{SS}$ ,  $\text{CaCO}_3$  and  $\delta^{13}\text{C}$  values indicating recurrent influxes of AABW glacial-style episodes with 4–6 kyr spacing. Maximum flow speed values and lowest  $\delta^{13}\text{C}$  values occur during MIS 10.4, indicating the level where full glacial conditions were reached.

#### 4.2. Climate Variability During MIS 11

[24] The duration of optimum climate conditions during interglacial MIS 11 has been discussed

controversially in the literature. Antarctic ice core records indicate that MIS 11 contains the longest (30 kyr) warm phase in Antarctic climate during the past 740 kyr [Siegenthaler *et al.*, 2005]. The absence of large fluctuations in  $\text{CO}_2$  and temperature suggests that stable warm climate conditions prevailed in Antarctica throughout the entire interval of 425–395 kyr. For the same time interval, stable climate conditions are also reflected in the Northern Hemisphere by the absence of ice-rafted debris and millennial-scale sea surface temperature (SST) variations in North Atlantic Ocean sediments [McManus *et al.*, 1999] and warm SST along the Iberian Margin [de Abreu *et al.*, 2005]. In contrast, marine benthic oxygen isotope values indicate maximum temperatures/minimum ice volume for a much shorter interval, recording heavier  $\delta^{18}\text{O}$  from  $\sim 400$  kyr on [Oppo *et al.*, 1998]. Modeling experiments link this early increase in



$\delta^{18}\text{O}$  to an early drop in deep ocean and Northern Hemisphere air temperature preceding the glacial inception [Bintanja *et al.*, 2005].

[25] The Site 1061  $\overline{\text{SS}}$  together with the benthic  $\delta^{13}\text{C}$  and  $\text{CaCO}_3$  records of both Sites 1061 and 1063 indicate that deep water conditions during the peak interglacial MIS 11.3 never attained stability (Figure 4). Flow speeds suggest that substantial changes in the position of the DWBC occurred throughout MIS 11 with distinct episodes of more vigorous flow associated with a shallower fast flowing core of the DWBC and lower NADW production. This interglacial variability is similar to earlier observations from ODP Site 980 located on the Feni Drift, east of Rockall Bank, Northeast Atlantic Ocean, where persistent millennial-scale ( $\sim 6$  kyr) variations in deep water circulation are recorded by benthic  $\delta^{13}\text{C}$  throughout the last 500 kyr, including MIS 11 [McManus *et al.*, 1999]. Such variability, which occurs regardless of the glacial state may suggest that the changes in the thermohaline circulation are not dominantly the result of meltwater-induced alteration of the deep convection [Broecker *et al.*, 1990; MacAyeal, 1993]. Rather as a development of the oscillator concept [Boyle and Keigwin, 1987; Oppo and Fairbanks, 1987; Duplessy *et al.*, 1988], McManus *et al.* [1999] suggested that North Atlantic overturning might not be balanced at an equilibrium level of salt and freshwater transport, but rather alternates between circulation schemes that export any excess of either one. As such, alteration between these modes can occur independent of the glacial state.

[26] However, we note that in comparison to the Site 980 benthic  $\delta^{13}\text{C}$  record, spectral analysis of the Site 1061  $\overline{\text{SS}}$  record shows deep flow variability during MIS 11 at a slightly higher periodicity at  $\sim 9$ –11 kyr. Indeed, this signal appears persistent throughout the entire interval of MIS 10–12, with perhaps the exception of late MIS 11 (Figure 5), and peak flow speeds are consistently accompanied by low benthic  $\delta^{13}\text{C}$  values at Site 1063 (Figure 4). Such variability with a 9–11 kyr periodicity may be of tropical origin and thus related to harmonic responses to precessional forcing at 11.5–, 10.4– and 9.5 kyr periods caused either by cross equatorial heat transport [Chapman *et al.*, 2000] or double insolation maximum and minimum in the tropics arising from the twice yearly passage of the sun across the equator [Hagelberg *et al.*, 1994; Berger *et al.*, 2006]. While such a forcing would occur regardless of the glacial state this would suggest a

direct linkage between surface processes in the subtropical northwestern Atlantic Ocean and deep circulation changes and should be traced in the surface water parameter as well. Indeed, Chaisson *et al.* [2002] traced a half precession signal in the difference between the  $\delta^{13}\text{C}$  values of *G. sacculifer* and *Neogloboquadrina dutertrei* at Site 1056 with maximum  $\Delta\delta^{13}\text{C}$  being linked with warmer, faster surges in the Gulf Stream. However, no such signal is apparent in the sea surface temperature reconstructions of the same core. Nonetheless, the 10 kyr filter of the Site 1061  $\overline{\text{SS}}$  record shows an in phase relationship with the  $\Delta\delta^{13}\text{C}$  of Site 1056 (not shown), so that we note a potential paradox in that Gulf Stream surges correspond to a shoaling/weakening of the DWBC, suggesting decreased lower LNADW production. While the coupling of Gulf Stream variability and the DWBC transport is poorly understood [e.g., Spall, 1996a, 1996b; Katsman *et al.*, 2001], our observation may point toward a combination of either stronger upper NADW circulation in response to the decreased LNADW production and/or enhanced wind-driven recirculation at these times.

### 4.3. Climate Deterioration After 397 kyr

[27] The marked increase in the intensity of millennial-scale (4–6 kyr) variability of the Site 1061  $\overline{\text{SS}}$  that characterize the transition from the peak interglacial MIS 11.3 (397 kyr) into MIS 10 parallels the general climate deterioration marked by the increased deposition of ice-rafted debris (IRD) at North Atlantic Site 980 (Figure 6a) [McManus *et al.*, 1999]. The episodic increases in flow speeds at Site 1061, consistent with a shallower glacial-like DWBC, appear to coincide with IRD maxima in the North Atlantic.

[28] Within dating uncertainties these episodic increases in flow speed values at Site 1061 are also accompanied by cooling events in the upper water column of BBOR, as indicated by increased  $\delta^{18}\text{O}$  values of *N. dutertrei* at Site 1056 [Chaisson *et al.*, 2002] and increased  $\delta^{18}\text{O}$  values of *Globigerinoides bulloides* from the Iberian Margin [de Abreu *et al.*, 2005] (Figures 6c and 6d) of which the latter has been shown to parallel IRD deposition at Site 980. Additionally, unpublished benthic  $\delta^{18}\text{O}$  and grain size records at the Iberian margin record high-amplitude variations in the strength of Mediterranean Outflow Water at times of decreased NADW formation (A. Voelker, personal communication, 2006) and presumably  $\overline{\text{SS}}$  variations at BBOR.

[29] Comparison of these different records (BBOR, Iberian Margin, Feni Drift) suggests that fluctuations at a 4–6 kyr timescale are widespread in the Northern Atlantic Ocean region and that surface and deep-ocean fluctuations may be essentially synchronous. This implies a similar coupling of North Atlantic ice rafting history and NADW export production as seen during the last glacial period and glacial-interglacial transition [e.g., Keigwin *et al.*, 1994; Sarnthein, 1994; Elliot *et al.*, 2002; McManus *et al.*, 2004; Hall *et al.*, 2006]. Most notably, the increasing intensity of millennial-scale variability in  $\overline{SS}$  occurs at  $\sim 3.8\%$  in the Site 1063 benthic  $\delta^{18}O$  and may be related to the transition of an ice volume threshold where climate variability is possibly amplified by feedback mechanisms associated with ice sheet growth [McManus *et al.*, 1999].

## 5. Conclusion

[30] Mean sortable silt grain-size has been used to reconstruct the intensity/position of the DWBC at Site 1061. A close relationship between the Site 1061  $\overline{SS}$  flow speeds and the benthic  $\delta^{13}C$  at Site GPC9 [Keigwin *et al.*, 1994] during MIS 5 strongly supports the interpretation of increased flow speeds at Site 1061 being associated with a shoaling of the deep fast flowing axis of the DWBC under reduced LNADW production conditions and incursions of southern sourced water to the area. These data are consistent with the core of the DWBC lying deeper than Site 1061 at present. A similar situation is observed during the peak interglacial MIS 11 and a shoaling to a more proximal position (higher  $\overline{SS}$ ) during the ice volume increase toward MIS 10, occurs in synchrony with changes in NADW production as shown from the benthic  $\delta^{13}C$  of Site 1063.

[31] We find evidence that variation in the position/strength of the DWBC at a 9–11 kyr pacing were generally persistent throughout MIS 10–12, thus independent of the glacial state. Such semiprecession variability may indicate a low-latitude origin for these changes. In addition, these data appear to agree with the glacial threshold hypothesis [McManus *et al.*, 1999] as the millennial-scale variability in  $\overline{SS}$  increases in the amplitude when  $\delta^{18}O$  values exceed  $\sim 3.8\%$ , but appear to be dampened somewhat when the value exceeds  $4.5\%$ . As noted by McManus *et al.* [1999], it is not unexpected that the presence and size of ice sheets should influence climate, given their affect on the atmospheric circulation and hydrologic

balance. Nonetheless, it remains an important goal to better understand the exact nature of the thresholds between different climate stability regimes.

## Acknowledgments

[32] We would like to thank Giancarlo Bianchi (GGB), Thomas Parry, and Helen Medley for their technical assistance. GGB is also thanked for extensive and useful discussions. Lucia de Abreu and Maria Serena Poli generously made their data available for comparison. We thank Jerry McManus and Mark Maslin, who provided constructive comments on an earlier version of this paper. This research used samples and/or data provided by the Ocean Drilling Program (ODP). ODP is sponsored by the U.S. National Science Foundation and participating countries (Natural Environment Research Council in UK) under management of Joint Oceanographic Institutions (JOI), Inc. This work was supported by funding from the UK National Environmental Research Council and UK Ocean Drilling Program.

## References

- Amos, A. F., A. L. Gordon, and E. D. Schneider (1971), Water masses and circulation patterns in the region of the Blake-Bahama Outer Ridge, *Deep Sea Res. Oceanogr. Abstr.*, *18*, 145–165.
- Bassiot, F. C., L. D. Labeyrie, E. Vincent, X. Quidellens, N. J. Shackleton, and X. Lancelot (1994), The astronomical theory of climate and the age of the Brunhes-Matuyama magnetic reversal, *Earth Planet. Sci. Lett.*, *126*, 91–108.
- Berger, A. L., and M. F. Loutre (1991), Insolation values for the climate of the last 10 million years, *Quat. Sci. Rev.*, *10*, 297–317.
- Berger, A. L., M. F. Loutre, and J. L. Melice (2006), Equatorial insolation: From precession harmonics to eccentricity frequencies, *Clim. Past*, *2*, 131–136.
- Bianchi, G. G., I. R. Hall, I. N. McCave, and L. Joseph (1999), Measurement of the sortable silt current speed proxy using the Sedigraph 5100 and Coulter Multisizer II: Precision and accuracy, *Sedimentology*, *46*, 1001–1014.
- Bianchi, G. G., M. Vautravers, and N. J. Shackleton (2001), Deep flow variability under apparently stable North Atlantic Deep Water production during the last interglacial of the subtropical NW Atlantic, *Paleoceanography*, *16*(3), 306–316.
- Bintanja, R., R. S. W. van de Wal, and J. Oerlemans (2005), Modelled atmospheric temperatures and global sea levels over the past million years, *Nature*, *437*, 125–128.
- Boyle, E. A., and L. D. Keigwin (1987), North Atlantic thermohaline circulation during the past 20,000 years linked to high-latitude surface temperature, *Nature*, *330*, 35–40.
- Broecker, W. S., G. Bond, and M. Klas (1990), A salt oscillator in the glacial Atlantic? 1. The concept, *Paleoceanography*, *5*, 469–477.
- Bryan, G. M. (1970), Hydrodynamic model of the Blake Outer Ridge, *J. Geophys. Res.*, *75*, 4530–4537.
- Chaisson, W. P., M. S. Poli, and R. C. Thunell (2002), Gulf Stream and Western Boundary Undercurrent variations during MIS 10–12 at Site 1056, Blake-Bahama Outer Ridge, *Mar. Geol.*, *189*, 79–105.
- Chapman, M. R., N. J. Shackleton, and J.-C. Duplessy (2000), Sea surface temperature variability during the last glacial-



- interglacial cycle: Assessing the magnitude and pattern of climate change in the North Atlantic, *Palaeogeogr. Palaeoclimatol. Palaeoecol.*, *157*, 1–25.
- de Abreu, L., F. F. Abrantes, N. J. Shackleton, P. C. Tzedakis, J. F. McManus, D. W. Oppo, and M. A. Hall (2005), Ocean climate variability in the eastern North Atlantic during interglacial marine isotope stage 11: A partial analogue to the Holocene?, *Paleoceanography*, *20*, PA3009, doi:10.1029/2004PA001091.
- Duplessy, J.-C., N. J. Shackleton, R. G. Fairbanks, L. Labeyrie, D. Oppo, and N. Kallel (1988), Deep-water source variations during the last climatic cycle and their impact on the global deep-water circulation, *Paleoceanography*, *3*, 343–360.
- Elliot, M., L. Labeyrie, and J.-C. Duplessy (2002), Changes in North Atlantic Deep-Water formation associated with the Dansgaard-Oeschger temperature oscillations (60–10 ka), *Quat. Sci. Rev.*, *21*, 1153–1165.
- EPICA Community Members (2004), Eight glacial cycles from an Antarctic ice core, *Nature*, *429*, 623–628.
- Ewing, J., M. Ewing, and R. Leyden (1966), Seismic profile survey of the Blake Plateau, *AAPG Bull.*, *50*, 1948–1971.
- Grützner, J., et al. (2002), Astronomical age models for Pleistocene drift sediments from the western North Atlantic (ODP Sites 1055 to 1063), *Mar. Geol.*, *189*, 5–23.
- Hagelberg, T. K., G. Bond, and P. deMenocal (1994), Milankovitch band forcing of sub-Milankovitch climate variability during the Pleistocene, *Paleoceanography*, *9*, 545–558.
- Hall, I. R., S. B. Moran, R. Zahn, P. C. Knutz, C.-C. Shen, and R. L. Edwards (2006), Accelerated draw-down of meridional overturning in the late-glacial Atlantic triggered by transient pre-H event freshwater perturbation, *Geophys. Res. Lett.*, *33*, L16616, doi:10.1029/2006GL026239.
- Haskell, B. J., and T. C. Johnson (1993), Surface sediment response to deepwater circulation on the Blake Outer Ridge, western North Atlantic: Paleoceanographic implications, *Sedimentol. Geol.*, *82*, 133–144.
- Haskell, B. J., T. C. Johnson, and W. J. Showers (1991), Fluctuations in deep western North Atlantic circulation on the Blake Outer Ridge during the last deglaciation, *Paleoceanography*, *6*, 21–31.
- Heezen, B. C., C. D. Hollister, and W. F. Ruddiman (1966), Shaping of the continental rise by deep geostrophic contour currents, *Science*, *152*, 502–508.
- Heslop, D., and M. J. Dekkers (2002), Spectral analysis of unevenly spaced climatic time series using CLEAN: Signal recovery and derivation of significance levels using a Monte Carlo simulation, *Phys. Earth Planet. Inter.*, *130*, 103–116.
- Hodell, D. A., K. A. Venz, C. D. Charles, and U. S. Ninnemann (2003), Pleistocene vertical carbon isotope and carbonate gradients in the South Atlantic sector of the Southern Ocean, *Geochem. Geophys. Geosyst.*, *4*(1), 1004, doi:10.1029/2002GC000367.
- Johns, E., R. A. Fine, and R. L. Molinari (1997), Deep flow along the western boundary of the Blake Bahama Outer Ridge, *J. Phys. Oceanogr.*, *27*, 2187–2208.
- Johnson, T. C., E. L. Lynch, W. J. Showers, and N. C. Placzuk (1988), Pleistocene fluctuations in the Western Boundary Undercurrent on the Blake Outer Ridge, *Paleoceanography*, *3*, 191–207.
- Katsman, C. A., S. S. Drijfhout, and H. A. Dijkstra (2001), The interaction of a Deep Western Boundary Current and the wind-driven gyres as a cause for low-frequency variability, *J. Phys. Oceanogr.*, *31*, 2321–2339.
- Keigwin, L. D., W. B. Curry, S. J. Lehman, and S. Johnsen (1994), The role of the deep ocean in North Atlantic climate changes between 70 and 130 kyr ago, *Nature*, *371*, 323–325.
- King, P., et al. (1998), Analysis of total and organic carbon and total nitrogen in settling oceanic particles and a marine sediment: An interlaboratory comparison, *Mar. Chem.*, *60*, 203–216.
- Laine, E. P., W. D. Gardner, M. J. Richardson, and M. A. Kominz (1994), Abyssal currents and advection of resuspended sediment along the north-eastern Bermuda Rise, *Mar. Geol.*, *119*, 159–171.
- Loutre, M.-F., and A. Berger (2003), Marine isotope stage 11 as an analogue for the present interglacial, *Global Planet. Change*, *36*, 209–217.
- MacAyeal, D. R. (1993), Binge/purge oscillations of the Laurentide Ice Sheet as a cause of the North Atlantic's Heinrich events, *Paleoceanography*, *8*, 775–784.
- McCartney, M. S., and L. D. Talley (1984), Warm water to cold water conversion in the northern North Atlantic Ocean, *J. Phys. Oceanogr.*, *14*, 922–935.
- McCave, I. N., and I. R. Hall (2006), Size sorting in marine muds: Processes, pitfalls, and prospects for paleoflow-speed proxies, *Geochem. Geophys. Geosyst.*, *7*, Q10N05, doi:10.1029/2006GC001284.
- McCave, I. N., and B. E. Tucholke (1986), Deep current-controlled sedimentation in the western North Atlantic, in *The Western North Atlantic*, edited by P. R. Vogt, and B. E. Tucholke, pp. 451–468, Geol. Soc. of Am., Boulder, Colorado.
- McCave, I. N., B. Manighetti, and S. G. Robinson (1995), Sortable silt and fine sediment size/composition slicing: Parameters for paleocurrent speed and paleoceanography, *Paleoceanography*, *10*(3), 593–610.
- McManus, J. F., D. W. Oppo, and J. L. Cullen (1999), A 0.5-million-year record of millennial-scale climate variability in the North Atlantic, *Science*, *283*, 971–975.
- McManus, J. F., R. Francois, J.-M. Gherardi, L. D. Keigwin, and S. Brown-Leger (2004), Collapse and rapid resumption of Atlantic meridional circulation linked to deglacial climate changes, *Nature*, *428*, 834–837.
- Oppo, D. W., and R. G. Fairbanks (1987), Variability in the deep and intermediate water circulation of the Atlantic Ocean during the past 25,000 years: Northern Hemisphere modulation of the Southern Ocean, *Earth Planet. Sci. Lett.*, *86*, 1–15.
- Oppo, D. W., J. F. McManus, and J. C. Cullen (1998), Abrupt climate change events 500,000 to 340,000 years ago: Evidence from subpolar North Atlantic sediments, *Science*, *279*, 1335–1338.
- Paillard, D., L. Labeyrie, and P. Yiou (1996), Macintosh program performs time-series analysis, *Eos Trans. AGU*, *77*, 379.
- Petit, J. R., et al. (1999), Climate and atmospheric history of the past 420,000 years from the Vostok ice core, Antarctica, *Nature*, *399*, 429–436.
- Poli, M.-S., R. C. Thunell, and D. Rio (2000), Millennial-scale changes in North Atlantic Deep Water circulation during marine isotope stages 11 and 12: Linkage to Antarctic climate, *Geology*, *28*, 807–810.
- Roberts, D. H., J. Lehar, and J. W. Dreher (1987), Time series analysis with CLEAN. 1. Derivation of a spectrum, *Astron. J.*, *93*, 968–989.
- Sarnthein, M. (1994), Changes in east Atlantic deepwater circulation over the last 30,000 years: Eight time slice reconstructions, *Paleoceanography*, *9*, 209–267.
- Schmitz, W. J. Jr., and M. S. McCartney (1993), On the North Atlantic circulation, *Rev. Geophys.*, *31*, 29–50.



- Shackleton, N. J., and M. A. Hall (1984), Oxygen and carbon isotope stratigraphy of Deep Sea Drilling Project Hole 552A: Plio-Pleistocene glacial history, *Initial Rep. Deep Sea Drill. Proj.*, *81*, 599–609.
- Shackleton, N. J., and N. D. Opdyke (1973), Oxygen isotope and paleomagnetic stratigraphy of Pacific core V28–238: Oxygen and isotope temperatures and ice volumes on a 105 and 106 year scale, *Quat. Res.*, *3*, 39–55.
- Shipboard Scientific Party (1998), Deep Blake-Bahama Outer Ridge, Sites 1060, 1061, and 1062, *Proc. Ocean Drill. Program Initial Rep.*, *172*, 157–250.
- Siegenthaler, U., et al. (2005), Stable carbon cycle-climate relationship during the late Pleistocene, *Science*, *310*, 1313–1317.
- Spall, M. A. (1996a), Dynamics of the Gulf Stream/Deep Western Boundary Current crossover. part I: Entrainment and recirculation, *J. Phys. Oceanogr.*, *26*, 2152–2168.
- Spall, M. A. (1996b), Dynamics of the Gulf Stream/Deep Western Boundary Current crossover. part II: Low-frequency internal oscillations, *J. Phys. Oceanogr.*, *26*, 2169–2182.
- Stahr, F. R., and T. B. Sanford (1999), Transport and bottom boundary layer observations of the North Atlantic Deep Western Boundary Current at the Blake Outer Ridge, *Deep Sea Res.*, *46*, 205–243.
- Torrence, C., and G. P. Compo (1998), A practical guide to wavelet analysis, *Bull. Am. Meteorol. Soc.*, *79*, 61–78.
- Weatherly, G. L., and E. A. Kelley (1984), Two views of the cold filament, *J. Phys. Oceanogr.*, *15*, 68–81.
- Yokokawa, M., and S.-O. Franz (2002), Changes in grain size and magnetic fabric at the Blake-Bahama Outer Ridge during the late Pleistocene (marine isotope stages 8–10), *Mar. Geol.*, *189*, 123–144.